

Asymmetry of the tidal tails of open star clusters in direct N -body integrations in Milgrom-law dynamics

J. Pflamm-Altenburg¹

Helmholtz-Institut für Strahlen- und Kernphysik, Nussallee 14-16, D-53115 Bonn e-mail: jpa@hiskp.uni-bonn.de

November 22, 2024

ABSTRACT

Context. Numerical QUMOND-simulations of star clusters orbiting in a Galactic disk potential show that the leading tidal arm of open star clusters contains tendentially more members than the trailing arm. However, these type of simulations are performed by solving the field-equations of QUMOND and already become non-practical for star cluster masses at around $5000 M_{\odot}$. Nearby star clusters have masses of $1000 M_{\odot}$ or ≈ 1000 particles and less/fewer and can currently not be simulated reliably in field-theoretical formulations of MOND.

Aims. The difference of the formation and evolution of tidal tails of open star clusters in the Newtonian and in the MONDian context is explored in the case of an equal-mass $n = 400$ particle cluster ($M_{\text{tot}} = 200 M_{\odot}$).

Methods. In order to handle particle numbers below the QUMOND-limit the star cluster is simulated in Milgrom-law dynamics (MLD): Milgrom's law $g_N = \mu(|a_M|/a_0)a_M$ is postulated to be valid for discrete systems in vectorial form. MLD shares the property with QUMOND that the acceleration of a particle outside any isolated mass concentration scales inversely with the distance. However, in MLD an internally Newtonian binary will follow a Newtonian rather than a MONDian path around the Galactic centre. In order to suppress the Newtonisation of compact subsystems in the star cluster the gravitational force is softened below particle distances of $0.001 \text{ pc} \approx 206 \text{ AU}$. Thus, MLD can only be considered as an approximation of a full MOND-theoretical description of discrete systems which are internally in the MOND regime. The MLD equations of motion are integrated by the standard Hermite scheme generally applied to Newtonian N -body systems, which is extended to solve for the accelerations and jerks associated with Milgrom's law.

Results. It is found that the tidal tails of a low-mass star cluster are populated asymmetrically in the MLD-treatment, very similar to the QUMOND simulations of the higher-mass star clusters. In the MLD-simulations the leading tail hosts up to twice as many members than the trailing arm and the low-mass open star cluster dissolves approximately 25% faster than in the respective Newtonian case. Furthermore, the numerical simulations show that the Newtonian integrals of motion are not conserved in MLD. However, the case of an isolated binary in the deep MOND limit can be handled analytically. The velocity of the Newtonian centre of mass does not increase continuously but wobbles around the constantly moving MLD centre of mass.

Key words. gravitation – Galaxies: star clusters: general – open clusters and associations: general – stars: kinematics and dynamics

1. Introduction

The rotation curves of disk galaxies are found to stay flat with increasing galactocentric radius. However, as the mass density decreases with increasing distance to the galactic centre the rotation curves were expected to fall (e.g. Rubin et al. 1978; Bosma 1981). This discrepancy has been attributed to the presence of un luminous (dark) matter. Candidates being part of the standard model of particle physics (e.g. brown dwarfs, white dwarfs and planetary objects have been continuously excluded (Bertone & Hooper 2018)). Thus, it has been concluded that the hypothesised dark matter consists of particles beyond the standard model of particle physics. However, the direct search for dark matter particles is still negative. Even previously reported positive signals (Aprile et al. 2020) could not be confirmed afterwards by the increased amount of measurement data (Aprile et al. 2022).

Considered as one of the strongest direct empirical evidence for the existence of dark matter are the two colliding galaxy clusters, called Bullet cluster 1E 0657-56, where an offset between the peaks in the X-ray mass distribution of hot intra cluster gas (Markevitch et al. 2002) and the peaks in the mass distribution obtained by weak-lensing observations has been claimed to be detected (Clowe et al. 2006). However, it has been mentioned

in Markevitch et al. (2002, Sec. 4.3) that the basic assumption of hydrostatic equilibrium required for the gas mass estimation can easily lead to an overestimate of the mass due to the high temperature during the collision. Furthermore, the fulfillment of the basic requirements for the determination of the X-ray masses has never been put to the test in the case of the Bullet cluster. In order to assume hydrostatic equilibrium the sound crossing time through the cluster needs to be shorter than the age of the system (e.g. Ettori et al. 2013, Sec. 2). This might be the case for an isolated single galaxy cluster with an age in order of a Hubble time $\approx 13 \text{ Gyr}$.

The more massive main cluster in the Bullet cluster has a temperature of about 14 keV, the less massive subcluster a temperature of about 6 keV (Clowe et al. 2006; Markevitch et al. 2002). Taking a very conservative radius of $\approx 0.2 \text{ Mpc}$ of each cluster and the claimed peaks the sound crossing times for each subcomponents lie between 0.24 Gyr and 0.36 Gyr and the sound crossing time of the entire system with an estimated radius of about 0.7 Mpc vary between 0.82 Gyr and 1.26 Gyr (Ettori et al. 2013, Eq. 4). Barrena et al. (2002) determined the age of the merger system to be about 0.15 Gyr by tracing the orbits of the individual clusters back to the time point of impact. Thus, the

requirement of hydrostatic equilibrium may be fulfilled by an isolated galaxy cluster but hardly by young merger systems like the Bullet cluster.

Furthermore, even if the derived X-ray gas distribution were true the standard argument that the hot plasma gas and the weak-lensing mass peaks are well separated from each other (eg. Drees 2019) is not entirely true. Table 2 in Clowe et al. (2006) lists four mass peaks of the hot X-ray gas of similar total gas mass, two of them associated with the hot peaks which are offset from the two clusters. The two other peaks are located at the respective brightest cluster galaxies.

As an alternative solution to the observed discrepancy between the observed distribution of matter in disk galaxies and their rotation curves Milgrom (1983c,a,b) proposed that the kinematical acceleration, a , is identical to the Newtonian gravitational acceleration, g , above a critical threshold $a_0 \approx 1.2 \times 10^{-10} \text{ m/s}^2 = 3.8 \text{ pc/Myr}^2$,

$$a = g, \quad (1)$$

and is proportional to the square root of the Newtonian gravitational acceleration below a_0 ,

$$a = \sqrt{a_0 G g}, \quad (2)$$

where $G = 0.0045 \text{ pc}^3/\text{M}_\odot \text{ Myr}^2$ is the gravitational constant. This concept is called Modified Newtonian Dynamics (MOND). The transition between the two regions is described by an interpolation function, $\mu(x)$, with properties

$$\mu(x) = \begin{cases} 1 & , \quad x \gg 1 \\ x & , \quad x \ll 1 \end{cases} \quad (3)$$

and $\mu'(x) > 0$, where the argument $x = a/a_0$ is the ratio of the absolute value of the kinematical acceleration and the threshold acceleration. Then, the relation between the kinematical and the gravitational acceleration is given by

$$\mu(a/a_0)a = g, \quad (4)$$

which is commonly referred to as Milgrom's law or in vectorial notation

$$\mu(|\mathbf{a}|/a_0)\mathbf{a} = \mathbf{g}. \quad (5)$$

Shortly after the formulation of Eq. (4) Felten (1984) pointed out that the direct application of Eq. (4) to the isolated two-body problem leads to a non-conservation of linear momentum. Such an unusual dynamical behavior is not surprising. As the gravitational acceleration, \mathbf{g} , on the right-hand side in Eq. (5) is a conservative field, the kinematical acceleration, \mathbf{a} , on the left-hand side is generally not conservative.

In order to ensure a conservative acceleration field Bekenstein & Milgrom (1984) extended the classical Poisson equation for the Newtonian potential, Φ_N ,

$$\Delta\Phi_N = 4\pi G\rho, \quad (6)$$

and formulated the AQUAL version of MOND,

$$\nabla \left(\mu \left(\frac{|\nabla\Phi_A|}{a_0} \right) \nabla\Phi_A \right) = 4\pi G\rho, \quad (7)$$

where ρ is the spatial mass density and Φ_A is the potential of the kinematical acceleration field with the relation $\mathbf{a} = -\nabla\Phi_A$. The AQUAL-Eq. (7) reduces to the vectorial form of Milgrom's law (Eq. (5)) only in cases of very high symmetry, e.g. in systems

with a spherically symmetric mass distribution or in thin axis-symmetric disks.

Due to the non-linearity of Eq. (7) obtaining analytic solutions is much more difficult than in the simpler Poissonian case. Milgrom (2010) formulated a quasi-linear version of MOND, where the differential part is identical to the Poissonian case but with a modified source term,

$$\Delta\Phi_Q = \nabla \cdot \left[\nu \left(\frac{|\nabla\Phi_N|}{a_0} \right) \nabla\Phi_N \right], \quad (8)$$

where the Newtonian potential is given by the standard Poisson equation Eq. (6).

Thus, the QUMOND equation is linear in the QUMOND-potential, Φ_Q , but non-linear in the corresponding Newtonian potential. Here, $\nu(y)$ is the transition function from the Newtonian to the MONDian regime with properties

$$\nu(y) = \begin{cases} 1 & , \quad y \gg 1 \\ 1/\sqrt{y} & , \quad y \ll 1 \end{cases} \quad (9)$$

in order to fulfill the observed boundary conditions in Eqs. (1,2).

If the hidden mass problem is due to a change of the gravitational or the dynamical laws in the weak acceleration regime, then deviations from the Newtonian dynamics are expected on small scales as well, for example in Globular and open star clusters. Stellar tidal tails of star clusters are expected to form symmetrically in Newtonian dynamics (eg. Küpper et al. 2010; Pflamm-Altenburg et al. 2023). Observations of the Galactic Globular cluster Pal 5 show asymmetries between both tidal arms (Ibata et al. 2017). This has been attributed to a disruptive encounter with a dark matter sub halo (Ercal et al. 2017) or a giant molecular cloud (Amorisco et al. 2016). In these cases, the observed asymmetry arises from a gap in previously symmetrically populated tidal tails. Contrary, in MONDian dynamics an asymmetry between both tidal tails arises naturally (Thomas et al. 2018).

Asymmetries between leading and trailing tidal arms have also been found in four open star clusters (Hyades, Coma Berenices, Praesepe and NGC 752) in the Solar vicinity (Jerabkova et al. 2021; Boffin et al. 2022; Beccari et al. in prep.). Dynamical interactions with a Galactic bar or spiral arms might cause local asymmetries in the tidal tails of open star clusters (Bonaca et al. 2020; Pearson et al. 2017, cf.). In three cases (Praesepe, Coma Berenices and NGC 752) the degree of the observed asymmetry can be explained by the stochastic nature of the evaporation of single stars through both Lagrange points. But in the case of the Hyades the random occurrence of the observed asymmetry would be a 6.7σ event (Pflamm-Altenburg et al. 2023). Contrary, the asymmetric tidal tails of the Hyades are a very likely result in MONDian dynamics (Kroupa et al. 2022).

The dynamical simulation of the evolution of the tidal tails of the Globular cluster Pal 5 (Thomas et al. 2018) and a massive open star cluster in the Galactic disk (Kroupa et al. 2022) have been done by use of the Phantom of Ramses code (PoR) (Lüghausen et al. 2015) which is an extension of the Ramses code (Teyssier 2002) and allows the dynamical simulations of systems containing gas and stars in the QUMOND-field formulation (Milgrom 2010).

Because MOND is formulated by the field theories AQUAL and QUMOND, numerical tools require a smooth mass density distribution. Therefore, star clusters are treated to be collisionless systems and energy redistribution between individual particles are not considered. Particles can only leave the cluster if

their effective energy in the co-rotating reference frame, where the star cluster is at rest, is large enough to pass through the Lagrange points and to overcome the tidal threshold. Stars having initially positive energy with respect to minimum energy required to escape from the cluster do not leave immediately the cluster but can be kept trapped by the star cluster up to a Hubble time (Fukushige & Heggie 2000). As energy redistribution between particles is not possible in collision-less N -body codes the upper region in the velocity distribution of stars is continuously depleted. However, the dynamics between the particles of discrete stellar systems repopulates the upper velocity region which leads to an enhanced evaporation. This special property of discrete stellar systems can only be modeled with a collisional code. The probability of escape from a star cluster is also effected by the orientation of the stellar orbit with the cluster (Read et al. 2006; Tiongco et al. 2016) and it might be possible that the process of energy redistribution among stars is different in Newtonian and MONDian dynamics and leads already to an asymmetric evaporation process. This kind of dynamical issues can never be explored by a collision-less code. Furthermore, the graininess of the mass distribution already leads to resolution limitation in the collision-less QUMOND modeling of a 5000 M_\odot star cluster (Kroupa et al. 2022).

It is the aim of this work to construct equations of motion for a discrete stellar system in MONDian dynamics and to study the formation and the evolution of tidal tails of low-mass star open clusters in this context. As equations of motion of a discrete stellar system are not available in the context of AQUAL and QUMOND the generalization of Milgrom's law is considered. In Sect. 2 the equations of motion of a discrete stellar system are formulated. Section 3 presents the numerical method to integrate the discrete equations of motion, which is an extension of the standard Hermite scheme used in direct Newtonian models. In Sect. 4 numerical tests of MLD are performed in order to explore the range of applicability and the limitation of this kind of MOND formulation. The results of the numerical simulations are presented in Sect. 5 where the formation and the evolution of stellar tidal tails of an open star cluster in the MONDian and the pure Newtonian case are compared with each other.

2. MLD equations of motion of a discrete stellar system

The direct application of Milgrom's law in order to calculate a MONDian acceleration from the Newtonian gravitational accelerations has been considered already in the past in a cosmological context (Nusser 2002; Knebe & Gibson 2004). The gravitational acceleration was calculated using the Poisson equation where the smooth mass density distribution is obtained by a particle-mesh method.

Here, this way is followed and we postulate the validity of Milgrom's law in Eq. (5) to be valid for discrete systems. The equations of motion of an isolated, discrete system of N gravitationally interacting particles are given by

$$\mu\left(\frac{|\mathbf{a}_i|}{a_0}\right)\mathbf{a}_i = G \sum_{\substack{j=0 \\ j \neq i}}^{j=N} \frac{m_j}{|\mathbf{r}_j - \mathbf{r}_i|^3} (\mathbf{r}_j - \mathbf{r}_i), \quad (10)$$

where m_j is the mass and \mathbf{r}_j the position vector of the j -th particle, \mathbf{r}_i the position vector and \mathbf{a}_i the acceleration vector of the i -th particle.

If a compact subsystem of n particles is considered, e.g., a star cluster in a galaxy, the right hand side in Eq. (10) is split into

two parts: i) the fully gravitationally self-interacting subsystem, ii) the embedding external gravitational mass, i.e., all particles with index $i > n$, acting as an external perturbative Newtonian potential, $\Phi_{\text{ext}}(\mathbf{r})$,

$$\mu\left(\frac{|\mathbf{a}_i|}{a_0}\right)\mathbf{a}_i = G \sum_{\substack{j=0 \\ j \neq i}}^{j=n} \frac{m_j}{|\mathbf{r}_j - \mathbf{r}_i|^3} (\mathbf{r}_j - \mathbf{r}_i) - \nabla\Phi_{\text{ext}}(\mathbf{r}_i). \quad (11)$$

This N -body formulation of MOND also shows an external field effect (EFE) in the case where the internal acceleration is smaller than the external kinematical acceleration a_{ext} . The scaling factor on the left-hand side in Eq. (11) is approximately a common constant factor $\mu(a_{\text{ext}}/a_0)$ and the equation of motion are effectively those of a Newtonian system with a rescaled effective gravitational constant $G_{\text{EFE}} = G/\mu(a_{\text{ext}}/a_0)$. For example the Pleiades open star cluster has a total stellar mass of about 740 M_\odot and a half-mass radius of $r_h = 3.66$ pc (Pinfield et al. 1998). Treating the Pleiades as a Plummer sphere (Plummer 1911) this corresponds to a Plummer parameter of $b = 2.8$ pc. In a Plummer sphere the maximum internal acceleration is $a_{\text{max}} = 2MG/\sqrt{27}b^2$ at a radial distance of $r_{\text{max}} = b/\sqrt{2}$ to the cluster centre. For the Pleiades the maximum acceleration is then 0.16 pc/Myr $^2 \approx a_0/24$ and evolves as a quasi-Newtonian system with an increased Gravitational constant.

As already mentioned in the Introduction the MONDian acceleration field is not conservative and the (classical) linear (Newtonian) momentum is not conserved (Felten 1984), which means that it can not be derived as the gradient of a scalar potential. However, if the physical origin of MONDian effects is due to an interplay between the vacuum and the gravitating masses (Milgrom 1999), conservation of extensive quantities would be expected to exist for the total system (vacuum plus gravitating mass) rather than for an effectively non-isolated subsystem. Furthermore, Felten (1984) restricted the discussion of momentum conservation to the isolated two-body problem in the deep MOND regime. Systems where direct tests of the conservation of linear momentum are accessible (surface of the earth and the solar system) have absolute acceleration well above the threshold acceleration, a_0 , and are in the deep Newtonian regime. The vacuum only acts as a very weak perturber and its influence is basically negligible and no violation of the conservation of linear momentum will be detectable. But if the system has absolute accelerations below a_0 then the vacuum might have a strong influence on the dynamical properties of the gravitating system and the mass points can not be considered as an isolated system anymore.

Furthermore, the non-existence of a scalar potential of the acceleration field in Eq. (5) does not imply that Eq. (10) is not equivalent to an Euler-Lagrange equation derivable from a Lagrangian. For instance, the equation of motion of a particle with mass m and charge q moving in an electric field \mathbf{E} and non-conservative magnetic field \mathbf{B} ,

$$m\ddot{\mathbf{q}} = q(\mathbf{E} + \dot{\mathbf{q}} \times \mathbf{B}), \quad (12)$$

can be derived from the Lagrangian

$$L = \frac{m}{2}\dot{\mathbf{q}}^2 - q(\Phi - \dot{\mathbf{q}} \bullet \mathbf{A}), \quad (13)$$

where \mathbf{A} is the vector potential of the magnetic field \mathbf{B} . As a second example the time-independent equation of motion of the damped harmonic oscillator

$$m\ddot{q} + \gamma m\dot{q} + \omega^2 q = 0 \quad (14)$$

can be derived from the Lagrangian

$$L = e^{\gamma t} \left(\frac{m}{2} \dot{q}^2 - \frac{\omega^2}{2} q^2 \right), \quad (15)$$

even though the system loses continuously energy due to a non-conservative frictional force ($\gamma < 0$), reflected by the explicit time-dependency of the Lagrangian.

Therefore, more theoretical work is required to explore if or to what extent Milgrom's law dynamics or related formulations can be expressed by a variational principle.

3. Numerical algorithm

As the numerical effort of integrating the Newtonian equations of motion of a self-gravitating discrete system scales to first order with the square of the particle number, these equations are generally integrated by use of the Hermite scheme (Aarseth 2003; Makino 1991; Kokubo et al. 1998; Hut et al. 1995) to reduce the number of function evaluations. The Hermite method makes use of the accelerations, \mathbf{a} , calculated by direct summation over all pairwise interactions and their time derivatives, $\mathbf{j} := \dot{\mathbf{a}}$ (called jerks), because the jerks can be obtained simultaneously during the calculation of the accelerations. In the following subsection the Hermite scheme, which is a predictor corrector method, is summarized.

3.1. Hermite scheme

Consider a particle at time t with position vector \mathbf{r} and velocity vector \mathbf{v} . In order to advance the particle in time with a time step of dt the acceleration vector \mathbf{a} and its time derivative $\mathbf{j} = \dot{\mathbf{a}}$ needs to be calculated at time t .

In the first sub-step (prediction) the position, \mathbf{r}_{pred} , and the velocity, \mathbf{v}_{pred} , are estimated at time $t + dt$ by a truncated Taylor expansion using the position, velocity, acceleration and jerk at time t

$$\mathbf{r}_{\text{pred}}(t + dt) = \mathbf{r}(t) + \mathbf{v}(t)dt + \frac{1}{2}\mathbf{a}(t)dt^2 + \frac{1}{6}\mathbf{j}(t)dt^3 \quad (16)$$

and

$$\mathbf{v}_{\text{pred}}(t + dt) = \mathbf{v}(t) + \mathbf{a}(t)dt + \frac{1}{2}\mathbf{j}(t)dt^2. \quad (17)$$

In the second sub-step the acceleration, \mathbf{a}_{pred} , and jerk, \mathbf{j}_{pred} , are calculated at time $t + dt$ using \mathbf{r}_{pred} and \mathbf{v}_{pred} .

In the third step the higher order terms of the Taylor expansion at time t

$$\mathbf{s} = \ddot{\mathbf{a}} = \frac{6(\mathbf{a}_{\text{pred}} - \mathbf{a})}{dt^2} - \frac{2(\mathbf{j}_{\text{pred}} + 2\mathbf{j})}{dt} \quad (18)$$

(called snap) and

$$\mathbf{c} = \ddot{\mathbf{j}} = \frac{12(\mathbf{a} - \mathbf{a}_{\text{pred}})}{dt^3} + \frac{6(\mathbf{j}_{\text{pred}} + \mathbf{j})}{dt^2} \quad (19)$$

(called crackle) are calculated.

In the fourth step the higher terms are added to the predicted position and velocity to obtain corrected values at the time $t + dt$

$$\mathbf{r}_{\text{corr}} = \mathbf{r}(t + dt) = \mathbf{r}_{\text{pred}} + \frac{1}{24}\mathbf{s}(t)dt^4 + \frac{1}{120}\mathbf{c}(t)dt^5 \quad (20)$$

and

$$\mathbf{v}_{\text{corr}} = \mathbf{v}(t + dt) = \mathbf{v}_{\text{pred}} + \frac{1}{6}\mathbf{s}(t)dt^3 + \frac{1}{24}\mathbf{c}(t)dt^4. \quad (21)$$

These corrected values are taken as new positions and velocities at time $t + dt$.

3.2. MONDian acceleration and jerk

First, the MONDian equations of motion (Eq. (11)) have to be solved for the acceleration. In Milgrom-law dynamics the Newtonian and the MONDian acceleration vectors are collinear. By introducing the unit acceleration vector \mathbf{e} it follows

$$\mu\left(\frac{|\mathbf{a}|}{a_0}\right)|\mathbf{a}|\mathbf{e} = |\mathbf{g}|\mathbf{e}. \quad (22)$$

Dividing by a_0 and setting

$$x = \frac{|\mathbf{a}|}{a_0}, \quad y = \frac{|\mathbf{g}|}{a_0} \quad (23)$$

$$\mu(x)x = y \quad (24)$$

emerges.

1. case, $y = 0$: It follows $x = 0$.

2. case, $y \neq 0$: The left hand side of Eq. (24) is an injective mapping from $\mathbb{R}_{>0}$ onto $\mathbb{R}_{>0}$. Therefore, a unique solution y exists. The solution can be obtained numerically in the general case. For some special forms of $\mu(x)$ Eq. (24) can be solved analytically for x . Then, the MONDian acceleration vector can be calculated by

$$\mathbf{a} = |\mathbf{a}|\mathbf{e} = xa_0\mathbf{e} = \frac{x}{y}ya_0\mathbf{e} = \frac{x}{y}|\mathbf{g}|\mathbf{e} = \frac{x}{y}\mathbf{g}. \quad (25)$$

The jerk, \mathbf{j} , of each particle can be calculated by differentiation of the MONDian acceleration with respect to the physical time. Differentiation of Eq. (5) leads to

$$\mu'\left(\frac{|\mathbf{a}|}{a_0}\right)\frac{\mathbf{a} \bullet \mathbf{j}}{a_0|\mathbf{a}|}\mathbf{a} + \mu\left(\frac{|\mathbf{a}|}{a_0}\right)\mathbf{j} = \dot{\mathbf{g}}. \quad (26)$$

This equation contains the jerk as a vector and as a part of a scalar product. By calculating the scalar product with \mathbf{a} we obtain an equation of $\mathbf{a} \bullet \mathbf{j}$ only which can be solved for it,

$$\mathbf{a} \bullet \mathbf{j} = \frac{\dot{\mathbf{g}} \bullet \mathbf{a}}{\mu'(x)x + \mu(x)}, \quad (27)$$

where the argument of the transition function is again $x = |\mathbf{a}|/a_0$. Finally, the jerk can be obtained from Eq. (26) after inserting the expression for $\mathbf{a} \bullet \mathbf{j}$

$$\mathbf{j} = \left(\dot{\mathbf{g}} - \frac{\mu'(x)}{\mu'(x)x + \mu(x)} \frac{\dot{\mathbf{g}} \bullet \mathbf{a}}{a_0|\mathbf{a}|}\mathbf{a} \right) \mu(x). \quad (28)$$

3.3. Newtonian case

The Newtonian case can be treated in the MONDian algorithm by setting the critical acceleration, a_0 , to a very small value. $a_0 = 10^{-20}$ Myr/pc² has been chosen in this work for this case. Then for $|\mathbf{a}| \gg a_0 \mu(x)$ tends to 1, $\mu'(x)$ tends to 0 and the MONDian values converge against the Newtonian values, $\mathbf{a} \rightarrow \mathbf{g}$ and $\mathbf{j} \rightarrow \dot{\mathbf{g}}$.

3.4. Transition function

In this work we use the transition function

$$\mu(x) = \frac{x}{\sqrt{1+x^2}}, \quad (29)$$

which is commonly referred to as the standard interpolation function (Famaey & McGaugh 2012), with derivative

$$\mu'(x) = \frac{1}{(1+x^2)^{3/2}}. \quad (30)$$

Eq. (24) can then be solved analytically,

$$x = \sqrt{\frac{y^2 + \sqrt{y^4 + 4y^2}}{2}}. \quad (31)$$

3.5. Newtonian acceleration and jerk with softening

In the Newtonian context the total (kinetic plus potential) energy of the individual stars follows a distribution function. Stars with positive total energy are able to escape from the star cluster and populate the tidal tails. This region of the energy distribution function is continuously repopulated due to energy redistribution among the remaining members of the star cluster. This energy gain is mainly due to numerous distant encounters between the stars. However, very close encounters occur rarely in open star cluster but pose numerical problems and require special algorithmic treatments (Aarseth 2003). In order to avoid these laborious implementations the singularity in the Newtonian potential, U_{ji} , between two point masses, m_j and m_i , is removed by adding a softening parameter, ε , to the distance of these particles (Aarseth 1963),

$$U_{ji} = -G \frac{m_j m_i}{|\mathbf{r}_{ji}|^2 + \varepsilon^2}. \quad (32)$$

Here, $\mathbf{r}_{ji} := \mathbf{r}_j - \mathbf{r}_i$ is the separation vector between the i -th and j -th particle. Then the total Newtonian acceleration, \mathbf{g}_i , of the i -th particle is given by summing over all pairwise softened gravitational force contributions

$$\mathbf{g}_i = G \sum_{\substack{j=0 \\ j \neq i}}^{j=n} \frac{m_j}{\left(|\mathbf{r}_{ji}|^2 + \varepsilon^2\right)^{3/2}} \mathbf{r}_{ji} + \mathbf{g}_{\text{ext},i}, \quad (33)$$

where $\mathbf{g}_{\text{ext},i}$ is the acceleration in the external field at the position of the i -th particle, \mathbf{r}_i . The corresponding softened Newtonian jerk is obtained by differentiation with respect to time,

$$\dot{\mathbf{g}}_i = G \sum_{\substack{j=0 \\ j \neq i}}^{j=n} \frac{m_j}{\left(|\mathbf{r}_{ji}|^2 + \varepsilon^2\right)^{3/2}} \left(\mathbf{v}_{ji} - 3 \frac{\mathbf{r}_{ji} \bullet \mathbf{v}_{ji}}{|\mathbf{r}_{ji}|^2 + \varepsilon^2} \mathbf{r}_{ji} \right) + \dot{\mathbf{g}}_{\text{ext}}, \quad (34)$$

where $\mathbf{v}_{ji} := \mathbf{v}_j - \mathbf{v}_i$ is the relative velocity vector between the particles j and i .

Additional to the numerical reason the softening accomplishes a physical purpose. In case of a very close subsystem the total particle accelerations are Newtonian and the μ -factor is unity. Thus, an internally Newtonian subsystem would follow a Newtonian orbit in the Galaxy rather than a MONDian orbit. Thus, the softening avoids the Newtonisation of close subsystems and sets a limitation of this method.

3.6. Galactic tidal field

For the Galactic tidal field an entirely flat rotation curve with a circular speed of $v_c = 225$ km/s, the same as in the related studies of open star clusters with asymmetric tidal tails (Jerabkova

et al. 2021; Pflamm-Altenburg et al. 2023), is chosen. The kinematical acceleration vector, \mathbf{a} , as a function of the Galactocentric distance, r , and in the case of a constant circular velocity, v_c , in the x - y -plane is

$$\mathbf{a} = -\frac{v_c^2}{r} \mathbf{e}_r = -\frac{v_c^2}{r^2} \mathbf{r}. \quad (35)$$

The required Newtonian acceleration, \mathbf{g}_{ext} , in order to keep a particle in MONDian dynamics on a circular path is

$$\mathbf{g}_{\text{ext}} = -\mu\left(\frac{v_c^2/r}{a_0}\right) \frac{v_c^2}{r^2} \mathbf{r}. \quad (36)$$

For the interpolating function chosen here (Eq. (29)) the explicit acceleration is

$$\mathbf{g}_{\text{ext}} = -\frac{v_c^4}{\sqrt{r^6 a_0^2 + r^4 v_c^4}} \mathbf{r} \quad (37)$$

and the corresponding Newtonian external jerk is

$$\dot{\mathbf{g}}_{\text{ext}} = -\frac{v_c^4}{\sqrt{r^6 a_0^2 + r^4 v_c^4}} \mathbf{v} + \frac{v_c^4 \mathbf{r} \bullet \mathbf{v} r^2 (3a_0^2 r^2 + 2v_c^4)}{(r^6 a_0^2 + r^4 v_c^4)^{3/2}} \mathbf{r}. \quad (38)$$

The Newtonian limit is again obtained by $a_0 \rightarrow 0$ and the external Newtonian acceleration converges against the right-hand side of Eq. (35).

4. Numerical tests of MLD

In order to get an insight what are the effects of this formulation of MOND, the dynamical behavior of special N -body systems are explored in this section before studying the formation and evolution of tidal tails in this dynamical context.

4.1. Isolated deep MOND binary

The first system considered is that of an isolated binary of non-equal mass constituents in the deep MOND regime. A binary with masses $m_1 = 2 M_\odot$ and $m_2 = 0.2 M_\odot$ is set up such that its semi-major axis would be $a = 1$ pc and eccentricity $e = 0.1$ in Newtonian dynamics with an orbital period of $T = \sqrt{\frac{4\pi^2 a^3}{G(m_1+m_2)}} = 63.15$ Myr. The minimum distance would be $r_{\text{min}} = a(1-e) = 0.9$ pc and therefore the maximum internal acceleration of the less-massive component is $g_{\text{max}} = Gm_1/r_{\text{min}}^2 = 0.01$ pc/Myr², which is two orders of magnitude smaller than a_0 . The initial conditions are $\mathbf{r}_1 = (-0.0818182, 0, 0)$ pc and $\mathbf{v}_1 = (0, -0.01, 0)$ pc/Myr for particle 1 and $\mathbf{r}_2 = (0.818182, 0, 0)$ and $\mathbf{v}_2 = (0, 0.1, 0)$ for particle 2. The binary is integrated with no softening ($\varepsilon = 0$).

In Newtonian dynamics stable and non-changing elliptical orbits are expected. In contrast, the left panel of Fig. 1 shows a slightly chaotic motion. The right panel reveals a regular pattern on a larger time-scale. The MOND binary seems not to be self-accelerated. This can be understood by inspection of the equation of motion. In the case that the system evolves in the deep MOND regime the general MLD-equation can be approximated by

$$\mathbf{a}_1 = \sqrt{Ga_0 m_2} \frac{\mathbf{q}_2 - \mathbf{q}_1}{|\mathbf{q}_2 - \mathbf{q}_1|^2} \quad (39)$$

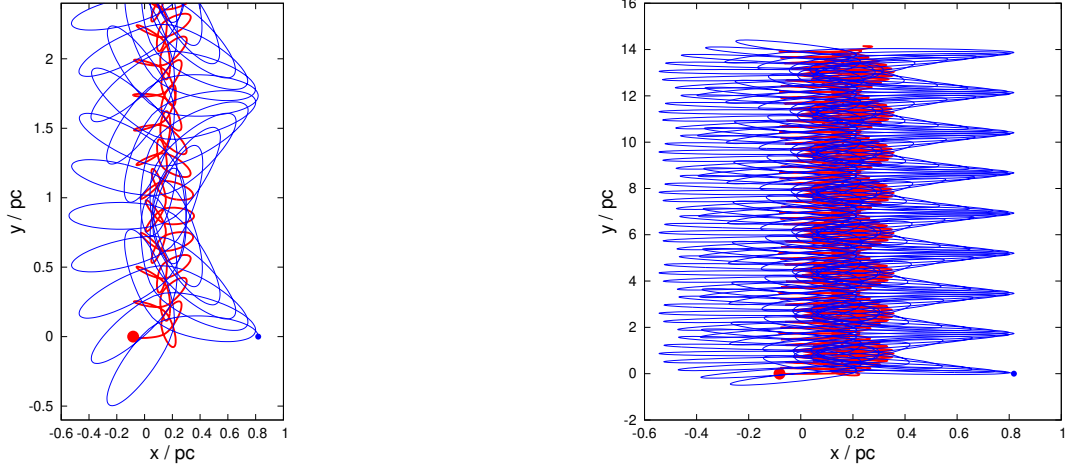


Fig. 1. Orbital evolution of a deep MOND MLD-binary: (*Left:*) The thick red curve shows the trajectory of the more massive particle with $m_1 = 2 M_\odot$, the thin blue curve shows the trajectory of the less massive particle with $m_1 = 0.2 M_\odot$. The large red filled circle indicates the initial position of the more massive particle, the small blue filled circle the initial position of the less massive particle. (*Right:*) Shown is the complete orbital evolution over a period of 1 Gyr.

$$\mathbf{a}_2 = -\sqrt{Ga_0 m_1} \frac{\mathbf{q}_2 - \mathbf{q}_1}{|\mathbf{q}_2 - \mathbf{q}_1|^2}. \quad (40)$$

It can be easily verified that these equations can be derived from the Lagrangian

$$L_{\text{MLD}} = \frac{\sqrt{m_1}}{2} \dot{\mathbf{q}}_1^2 + \frac{\sqrt{m_2}}{2} \dot{\mathbf{q}}_2^2 - \sqrt{Ga_0 m_1 m_2} \ln(|\mathbf{q}_2 - \mathbf{q}_1|). \quad (41)$$

Comparing with the Newtonian Lagrangian,

$$L_{\text{N}} = \frac{m_1}{2} \dot{\mathbf{q}}_1^2 + \frac{m_2}{2} \dot{\mathbf{q}}_2^2 + Gm_1 m_2 \frac{1}{|\mathbf{q}_2 - \mathbf{q}_1|}, \quad (42)$$

two changes can be seen. The Keplerian potential is replaced by a logarithmic potential and the masses of the particles in the kinetic potential turn into their square roots. Furthermore, inert and heavy mass are still equal.

Additionally, both Lagrangians share the same symmetries and are time-independent. The translational symmetry leads to the conservation of the MLD-momentum

$$\mathbf{p}_{\text{MLD}} = \sqrt{m_1} \dot{\mathbf{q}}_1 + \sqrt{m_2} \dot{\mathbf{q}}_2 = \text{const.} \quad (43)$$

Figure 2 shows that the Newtonian linear momentum does not increase continuously as the term self-acceleration might suggest, but oscillates around a constant value. The MLD-linear momentum oscillates very much weaker. It is not expected to stay constant as the binary evolves in the deep MOND regime, but the MLD-equations of motion converge only asymptotically against the Eqs. (39) and (40) for $\Delta q \rightarrow \infty$.

The motion in space of the binary system can be obtained by considering a transformation generated by a boost of a velocity \mathbf{v} ,

$$\mathbf{q}'_i(\varepsilon) = \mathbf{q}_i + \varepsilon \mathbf{v} t, \quad t' = t. \quad (44)$$

This leads to an invariant action and the quantity

$$I = \left(\sqrt{m_2} \dot{\mathbf{q}}_1 \cdot \mathbf{v} + \sqrt{m_2} \dot{\mathbf{q}}_2 \cdot \mathbf{v} \right) t - \left(\sqrt{m_1} \mathbf{v} \cdot \mathbf{q}_1 + \sqrt{m_2} \mathbf{v} \cdot \mathbf{q}_2 \right) \quad (45)$$

is conserved for all boosts \mathbf{v} . After division by $(\sqrt{m_1} + \sqrt{m_2})$ a MLD-expression of a centre of mass emerges

$$\mathbf{R}_{\text{com,MLD}} = \frac{\sqrt{m_1} \mathbf{q}_1 + \sqrt{m_2} \mathbf{q}_2}{\sqrt{m_1} + \sqrt{m_2}}, \quad (46)$$

which moves with constant speed and constant direction (Fig. 3), whereas the Newtonian centre of mass wobbles around the MLD-centre of mass.

Rotational symmetry leads to the conservation of the angular momentum

$$\mathbf{L}_{\text{MLD}} = \sqrt{m_1} \mathbf{q}_1 \times \dot{\mathbf{q}}_1 + \sqrt{m_2} \mathbf{q}_2 \times \dot{\mathbf{q}}_2 = \text{const.} \quad (47)$$

The evolution of the z -component of the Newtonian angular momentum which oscillates increasingly with time is shown in Fig. 4, whereas the MLD angular momentum is almost conserved.

The canonical momentum in MLD is

$$\mathbf{p}_i = \frac{\partial L_{\text{MLD}}}{\partial \dot{\mathbf{q}}_i} = \sqrt{m_i} \dot{\mathbf{q}}_i \quad (48)$$

and the associated Hamiltonian is

$$H_{\text{MLD}} = \frac{\mathbf{p}_1^2}{2\sqrt{m_1}} + \frac{\mathbf{p}_2^2}{2\sqrt{m_2}} - \sqrt{Ga_0 m_1 m_2} \ln(|\mathbf{q}_2 - \mathbf{q}_1|) = \text{const.} \quad (49)$$

which is time-independent and is therefore conserved. In this particular case both Hamiltonians oscillate (Fig. 5). However, the time evolution show no secular evolution.

4.2. Binaries in an external galactic field

As a next test the internally MONDian binary from Sec. 4.1 is put on a circular orbit with radius $R = 8300$ pc in a flat rotation curve with $v_c = 225$ km/s = 230 pc/Myr. The external acceleration is $a_{\text{ext}} = 6.37$ pc/Myr² (Eq. 35) and the corresponding Newtonian external acceleration is $g_{\text{ext}} = 5.47$ pc/Myr² (Eq. 36) and therefore about two orders of magnitude larger than the internal acceleration. Adding the kinematical circular velocity of 230 pc/Myr to both components in Galactic tangential direction

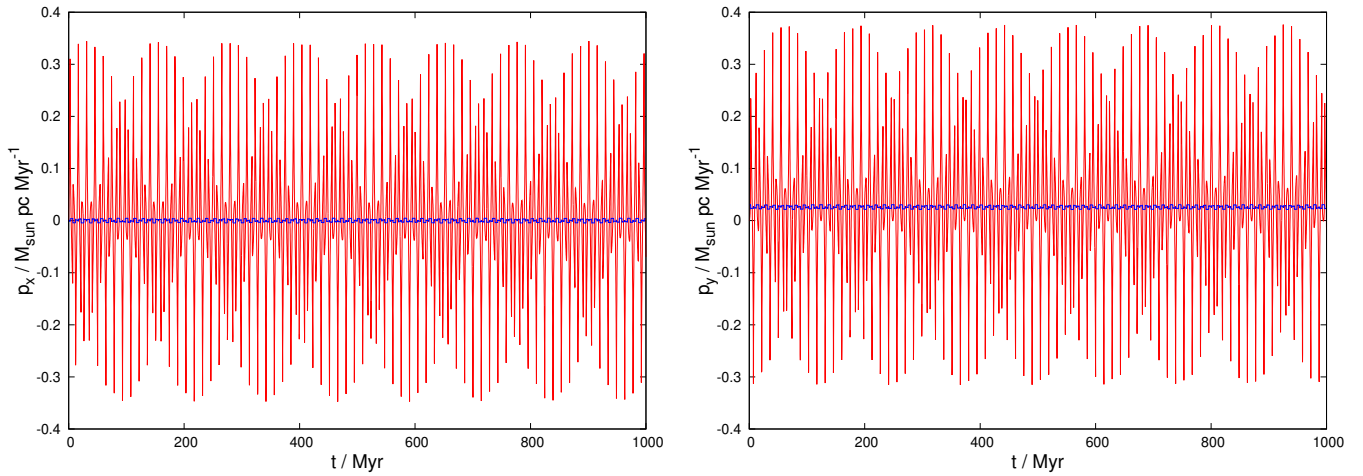


Fig. 2. Evolution of the linear momentum of a deep MOND MLD-binary: The slightly varying blue curve shows the MLD-linear momentum (Eq. (43)) as a function of time. The strongly oscillating red curve shows the time evolution of the corresponding Newtonian linear momentum, $\mathbf{p}_{\text{New}} = m_1 \dot{\mathbf{q}}_1 + m_2 \dot{\mathbf{q}}_2$. (Left): x -component of the linear momentum. (Right): y -component of the linear momentum.

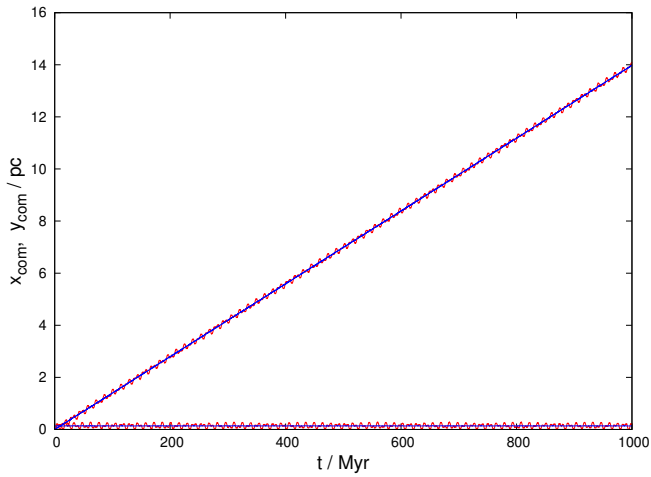


Fig. 3. Centre of mass motions. The straight blue lines refer to the MLD-centre of mass (Eq. (46)) whereas the wobbling red curves show the Newtonian centre of mass, $\mathbf{R}_{\text{com,New}} = \frac{m_1 \mathbf{q}_1 + m_2 \mathbf{q}_2}{m_1 + m_2}$. The x -component of both centers of mass runs horizontally, the y -component increases continuously.

leads to a circular Galactic motion of the internally MONDian binary (Fig. 6) with one Galactic revolution within 227 Myr. The binary is integrated with no softening ($\varepsilon = 0$).

The MLD-equation of motion of both binary components can be approximated by

$$\mu \left(\frac{a_{\text{ext}}}{a_0} \right) \mathbf{a}_1 = \frac{Gm_2}{|\mathbf{r}_2 - \mathbf{r}_1|^2} (\mathbf{r}_2 - \mathbf{r}_1) + \mathbf{g}_{\text{ext}} \quad (50)$$

$$\mu \left(\frac{a_{\text{ext}}}{a_0} \right) \mathbf{a}_2 = -\frac{Gm_1}{|\mathbf{r}_2 - \mathbf{r}_1|^2} (\mathbf{r}_2 - \mathbf{r}_1) + \mathbf{g}_{\text{ext}} \quad (51)$$

in case if the external acceleration is very much larger than the internal acceleration, $\mathbf{a}_{\text{ext}} \gg \mathbf{a}_{\text{int}}$.

For the acceleration of the Newtonian centre of mass follows

$$\frac{m_1 \mathbf{a}_1 + m_2 \mathbf{a}_2}{m_1 + m_2} = \frac{\mathbf{g}_{\text{ext}}}{\mu(a_{\text{ext}}/a_0)}, \quad (52)$$

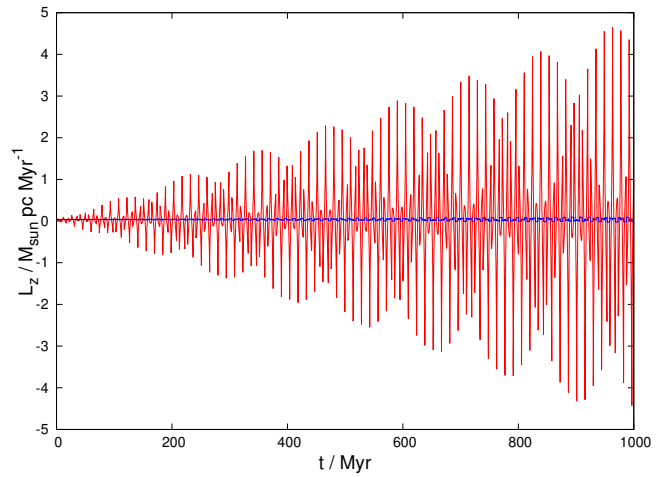


Fig. 4. Evolution of the angular momentum of a deep MOND MLD-binary: The slightly varying blue curve shows the MLD-angular momentum (Eq. (47)) as a function of time. The strongly oscillating red curve shows the time evolution of the corresponding Newtonian angular momentum, $\mathbf{L}_{\text{New}} = m_1 \mathbf{q}_1 \times \dot{\mathbf{q}}_1 + m_2 \mathbf{q}_2 \times \dot{\mathbf{q}}_2$.

and the radial acceleration is given by the scaled Newtonian acceleration.

In the next step an internally Newtonian binary with the same components is set up with a semi major axis of 2×10^{-3} pc with the same tangential velocity of 230 pc/Myr. The binary does not move on a circular orbit as seen in Fig. 7. A circular MONDian velocity of 230 pc/Myr corresponds to a Newtonian circular velocity of 213 pc/Myr at a Galactocentric distance of 8300 pc. Now, the binary moves on a circular orbit (Fig. 8). An internally Newtonian binary follows a Newtonian orbit.

4.3. Isolated hierarchical triple

An equal mass hierarchical triple is integrated in Newtonian dynamics and MLD, where the higher configuration is a MONDian binary with a semi-major axis of 1 pc and eccentricity $e = 0$. One component is a compact Newtonian binary with a semi-major axis of 10^{-3} pc and eccentricity $e = 0$. All three components have equal masses, $m_1 = m_2 = m_3 = 1 M_{\odot}$. Thus, the internal

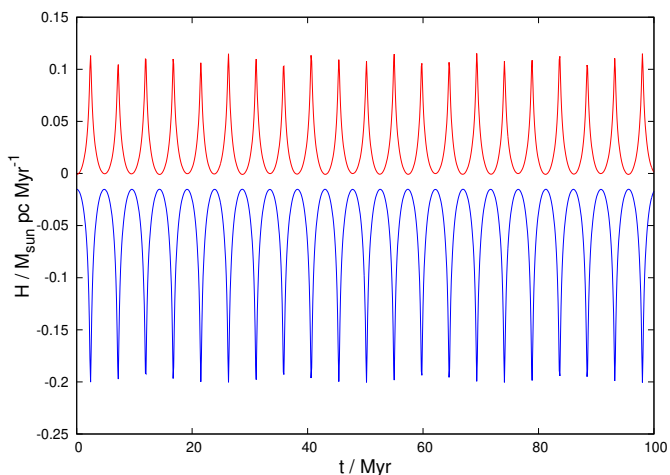


Fig. 5. Evolution of the Hamiltonian of a deep MOND MLD-binary: The blue curve shows the MLD-Hamiltonian (Eq. (49)) as a function of time. The red curve shows the time evolution of the corresponding Newtonian Hamiltonian, $H_{\text{New}} = \frac{\mathbf{p}_1^2}{2m_1} + \frac{\mathbf{p}_2^2}{2m_2} - G \frac{m_1 m_2}{|\mathbf{q}_2 - \mathbf{q}_1|}$.

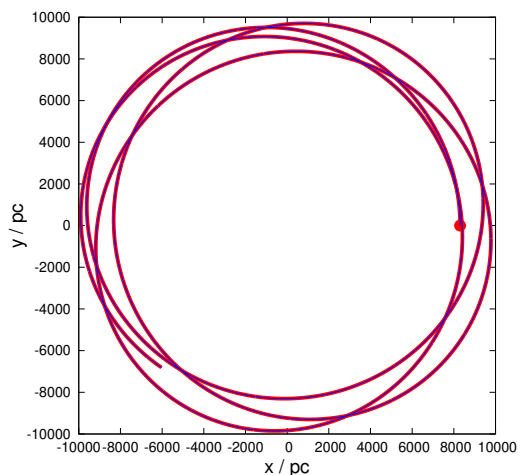


Fig. 7. Binary in an external field. The internally Newtonian binary is set up with a MONDian rotational velocity. The thick red curve shows the orbit of the $2 M_{\odot}$ -component, the thin blue curve shows the orbit of the less massive star. The filled red circle marks the initial position of the binary.

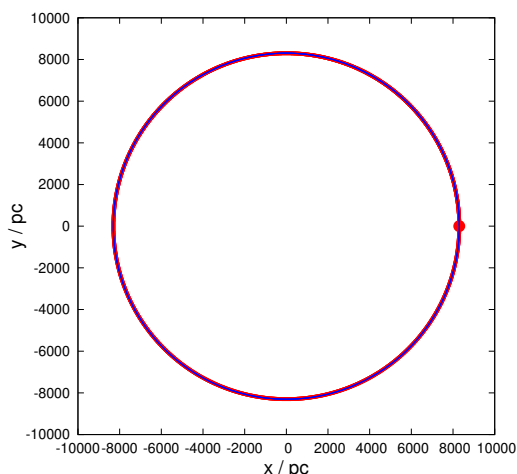


Fig. 6. Binary in external field. The internally MONDian binary follows the MONDian Galactic orbit. The thick red curve shows the orbit of the $2 M_{\odot}$ -component, the thin blue curve shows the orbit of the less massive star. The filled red circle marks the initial position of the binary.

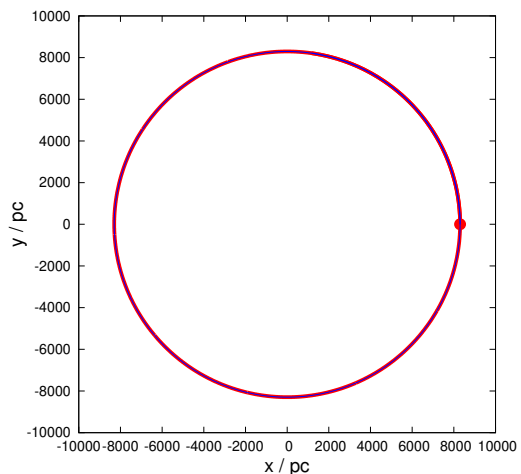


Fig. 8. Binary in an external field. The internally Newtonian binary is set up with a Newtonian rotational velocity. The thick red curve shows the orbit of the $2 M_{\odot}$ -component, the thin blue curve shows the orbit of the less massive star. The filled red circle marks the initial position of the binary.

Newtonian binary is an equal-mass binary, the outer one is a non-equal-mass binary. The initial conditions of the compact binary are $\mathbf{r}_1 = (-0.333833, 0, 0)$ pc, $\mathbf{v}_1 = (0, -1.53826, 0)$ pc/Myr and $\mathbf{r}_2 = (-0.332833, 0, 0)$ pc, $\mathbf{v}_2 = (0, 1.46083, 0)$ pc/Myr. The initial conditions of the third body are $\mathbf{r}_3 = (0.666667, 0, 0)$ pc, $\mathbf{v}_3 = (0, 0.0774363, 0)$ pc/Myr. The initial conditions are such that the Newtonian centre of mass is initially at rest at the origin. The internal Newtonian acceleration of the compact binary is $a_{\text{in}} = 4500 \text{ pc/Myr}^2 = 1184 a_0$. The acceleration of the less massive component of the outer binary is $a_{\text{out}} = 0.009 \text{ pc/Myr}^2 = 0.0024 a_0$. The triple system is integrated for 100 Myr with no softening ($\epsilon = 0$).

Figure 9 shows the orbital evolution of the triple system integrated in Newtonian dynamics. As expected both outer components move on circular orbits as it has no eccentricity. The centre of mass remains at rest. The evolution of the triple system in MLD is shown in Fig. 10. The orbital configuration now precesses around the origin. No net self-acceleration is visible.

4.4. Isolated Plummer sphere

A Plummer sphere (Plummer 1911; Aarseth et al. 1974) is set up with $n = 400$ particles with masses, $m_i = m_1 + (i-1)\Delta m$, equally distributed from $m_1 = 0.1 M_{\odot}$ and $m_n = 2 M_{\odot}$, with a mass difference of $\Delta m = (m_n - m_1)/(n-1)$. The total mass is $M_{\text{tot}} = n(m_n + m_1)/2 = 420 M_{\odot}$. Choosing a Plummer parameter of $b = 3.1$ pc the maximum internal acceleration is $0.076 \text{ pc/Myr}^2 = 0.02 a_0$. Figure 11 shows the evolution with time of the three spatial components of the Newtonian centre of mass. In lack of a known conserved quantity in MLD the MONDian simulation is here compared with a Newtonian simulation with identical initial conditions.

In the general N -body case it is currently not clear, if the MLD equations of motion can be derived from a variational principle and therefore the search for conserved quantities is much more difficult. However, a generalized expression of action equal reaction can be derived from Eq. (10) by multiplication with the

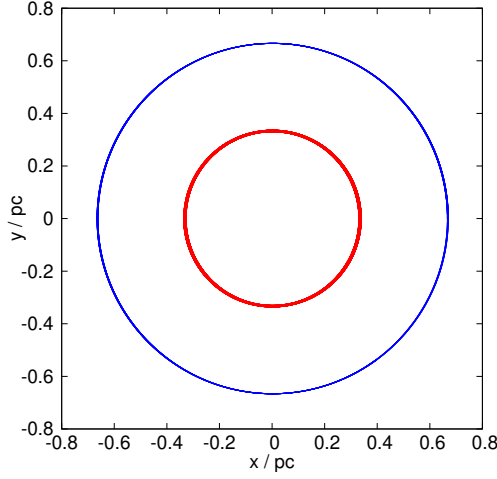


Fig. 9. Triple in Newtonian dynamics. The inner thick (red) circle shows the orbit of the inner more massive binary. The thin (blue) outer circle shows the orbit of the single star.

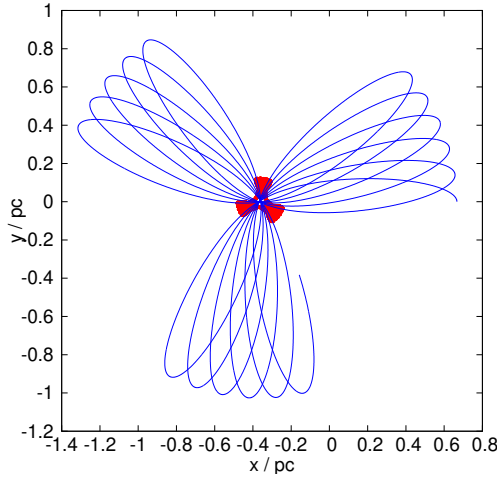


Fig. 10. Triple in MLD. The inner thick (red) circle shows the orbit of the inner more massive binary. The thin (blue) outer circle shows the orbit of the single star.

mass of the considered particle and by subsequent summation over all particles:

$$\sum_{i=1}^{i=N} m_i \mu \left(\frac{|\mathbf{a}_i|}{a_0} \right) \mathbf{a}_i = G \sum_{\substack{j,i=0 \\ j \neq i}}^{j,i=N} \frac{m_i m_j}{|\mathbf{r}_j - \mathbf{r}_i|^3} (\mathbf{r}_j - \mathbf{r}_i) = 0. \quad (53)$$

In the Newtonian limit the acceleration term can be expressed as the time derivative of the kinematical velocity

$$0 = \sum_{i=1}^{i=N} m_i \mathbf{a}_i = \sum_{i=1}^{i=N} m_i \dot{\mathbf{v}}_i = \frac{d}{dt} \sum_{i=1}^{i=N} m_i \mathbf{v}_i, \quad (54)$$

and the total Newtonian linear momentum is conserved.

4.5. Comparison with deep MOND two-body expressions

Milgrom (2014, E.q 23) concluded that any MOND field theory leads to an internal force of an isolated two-body system with masses m_1 and m_2 in the deep MOND limit of

$$F = \frac{2\sqrt{a_0 G}}{3r_{21}} \left((m_1 + m_2)^{3/2} - m_1^{3/2} - m_2^{3/2} \right), \quad (55)$$

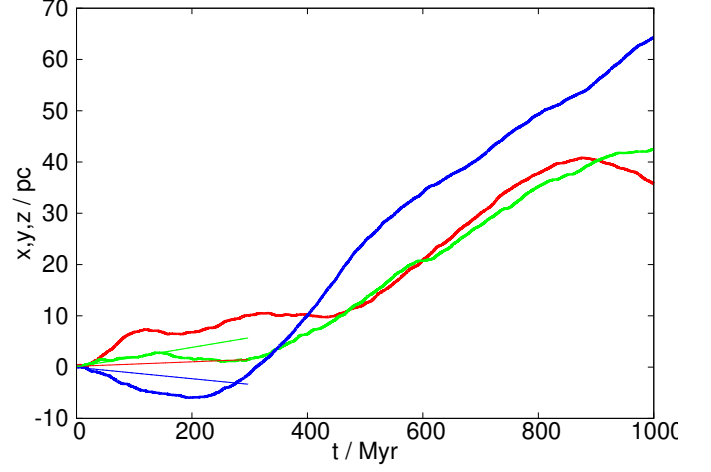


Fig. 11. Centre of mass evolution of an isolated MLD-Plummer sphere: The thick lines show the x -(red), y -(green) and z -(blue) component of the Newtonian centre of mass evolution with time of an isolated Plummer sphere in MLD. The thin lines show the evolution of the Newtonian centre of mass of a Plummer sphere in Newtonian dynamics with identical initial conditions as the MLD-Plummer sphere (with identical color-coding of the spatial components).

where r_{21} is the interparticle distance. Given that Newtonian momentum should be conserved in a MOND field theory (Bekenstein & Milgrom 1984) $m_1 \dot{\mathbf{r}}_1 = -m_2 \dot{\mathbf{r}}_2$ the equations of motion of both particles are

$$\dot{\mathbf{r}}_1 = \frac{2\sqrt{a_0 G}}{3m_1} \left((m_1 + m_2)^{3/2} - m_1^{3/2} - m_2^{3/2} \right) \frac{\mathbf{r}_2 - \mathbf{r}_1}{|\mathbf{r}_2 - \mathbf{r}_1|^2} \quad (56)$$

and

$$\dot{\mathbf{r}}_2 = -\frac{2\sqrt{a_0 G}}{3m_2} \left((m_1 + m_2)^{3/2} - m_1^{3/2} - m_2^{3/2} \right) \frac{\mathbf{r}_2 - \mathbf{r}_1}{|\mathbf{r}_2 - \mathbf{r}_1|^2} \quad (57)$$

The evolution of the relative orbit is shown in Fig. 12 in comparison to the MLD-equations for a duration of 20 Myr. In deep MOND the binary following the Milgrom (2014) equations of motion has got a slower motion in radial direction, but precesses slightly faster than the MLD-binary.

5. Tidal tail simulations of open star clusters

In order to explore the difference in the dynamical formation and evolution of tidal tails of open star clusters, low-mass star cluster models are set up on a circular orbit in a Galactic field with a flat rotation curve and are integrated with the algorithm presented in Sect. 3.

5.1. Initial conditions

The model star clusters contain 400 equal-mass point particles with a mass of $0.5 M_\odot$ each, which are constant in time, i.e. stellar evolution is not included. Thus, all models have a total mass of $200 M_\odot$. The particles are set up in phase space as a Plummer model (Plummer 1911; Aarseth et al. 1974) with a Plummer parameter of 3.1 pc. This corresponds to the properties of the current Hyades star cluster (Röser et al. 2019).

The initial position and velocity vectors of the star clusters are chosen such that their centre of mass orbits on a circular path with radius $r_0 = 8300$ pc in a flat rotation curve with 225 km/s,

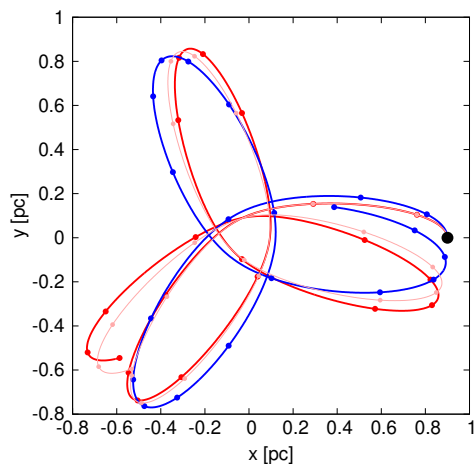


Fig. 12. Deep MOND binary. Shown is the relative motion over 20 Myr of the isolated test binary with initial conditions (filled black circle) given at the beginning of Sec. 4.1 for three different sets of equations of motion: full MLD with transition function (red solid line), MLD in the deep MOND limit (Eqs. 39 and 40, light red line), and Milgrom’s formulation (blue solid line, Eqs. 56 and 57). The small filled circles show the orbital positions in steps of 2 Myr.

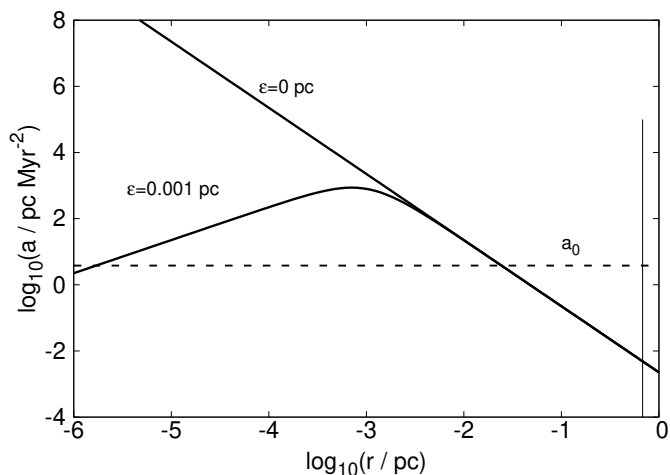


Fig. 13. Softening. Shown is the Newtonian acceleration field of a star with a mass of $0.5 M_{\odot}$ in the case of no softening ($\varepsilon = 0$ pc) and softening with a parameter of $\varepsilon = 0.001$ pc. The dashed horizontal line marks the MONDian acceleration threshold, a_0 . The vertical solid line indicates the mean central particle distance of ≈ 0.7 pc for a 400 particle Plummer sphere with Plummer parameter 3.1 pc.

similar to the solar neighborhood as used in related studies (Jerabkova et al. 2021; Pflamm-Altenburg et al. 2023)

The smoothing parameter is set to $\varepsilon = 10^{-3}$ pc. The difference between the softened and the unsoftened acceleration field of a particle with a mass of $0.5 M_{\odot}$ is shown in Fig. 13. The softened and the unsoftened acceleration fields start to diverge from each other at an acceleration of about 100 times higher than the MONDian threshold. The central particle density of the Plummer sphere is $n_0 = (3N/4\pi b^3)$ corresponding to a mean central inter particle distance of $\bar{d} \approx 0.7$ pc. Therefore, we expect that i) the driving long-distance encounters responsible for energy redistribution and the consequent evaporation of stars from the star cluster and ii) the difference between MONDian and Newtonian dynamics below the acceleration threshold, a_0 , are mostly unaffected by the gravitational softening.

In order to compare the MONDian and the Newtonian models, the threshold value is $a_0 = 3.8 \text{ Myr/pc}^2$ for the MONDian Models, and $a_0 = 3.8 \times 10^{-20} \text{ Myr/pc}^2$ for the Newtonian models. In total 10 (5 MONDian and 5 Newtonian) models are calculated. Two each models (1 Newtonian and 1 MONDian) are created with the same random seed and have identical initial conditions.

5.2. Time evolution of the orbital snapshots

The time evolution of one pair of star clusters in Newtonian and ML-dynamics is displayed in Fig. 14 at 0 Myr, in Fig. 15 after 250 Myr, in Fig. 16 after 500 Myr, in Fig. 17 after 750 Myr, and in Fig. 18 after 1000 Myr. In order to compare the relative positions of the star clusters in Newtonian and ML-dynamics, the arrows indicating the direction of the Galactic rotation and the direction to the Galactic centre and the corresponding labels are located at the same position. The short dashed line indicates the path from the Galactic centre to the density centre of the star cluster and the solid curved line shows the circular orbit.

The star clusters orbit anti-clockwise. The inner arm is the leading arm, the outer arm is the trailing arm. In the Newtonian case both tidal arms are approximately equally populated. In the MLD case the tidal tails are populated asymmetrically. The leading tidal arm contains continuously more members than the trailing arm.

Simultaneously to the asymmetric population of the tidal arms in ML-dynamics, the star cluster follows the Newtonian star cluster. This can be seen in the larger separation between the arrow pointing towards the Galactic centre and the connecting (dashed) line between the Galactic centre and the density centre of the star cluster in the MLD case than in the Newtonian case.

This might be due to some kind of local conservation of linear momentum. As more stars end up in the leading tail, more momentum is carried away from the star cluster into the moving direction of the star cluster. Thus, the star cluster is expected to get a small recoil. However, as pointed out in Sect. 2 a concept like linear momentum conservation as in Newtonian dynamics does not exist in Milgrom-law dynamics. Further theoretical work is required in order to explore the conservation of dynamical quantities in MLD.

5.3. Analyzing the tidal tails

The criterion whether or not a star is considered to be a member of the star cluster or of the leading/trailing tidal arm is the same as in Pflamm-Altenburg et al. (2023). If the distance of a star to the centre of the star cluster is less than a cut of radius (here 10 pc) then the star is considered to be a member of the star cluster. If this distance is larger than 10 pc then the star is considered to be a member of one tidal arm. If the angle between the distance vector of the particular star to the star cluster centre and the velocity vector of the star cluster is less than 90° then the star is considered to be a member of the leading tidal arm. If this angle is larger than 90° the star is assigned to the trailing arm.

In Pflamm-Altenburg et al. (2023) the stochastic asymmetry of tidal tails in Newtonian dynamics has been quantified using test particle calculations in an analytic Plummer potential orbiting the Galactic centre. The origin of the Plummer potential has been used as the cluster centre. In this work the cluster centre has to be determined by the positions of all particles following standard procedures. A local density is assigned to each particle using the 6-th nearest neighbour method (Casertano & Hut 1985).

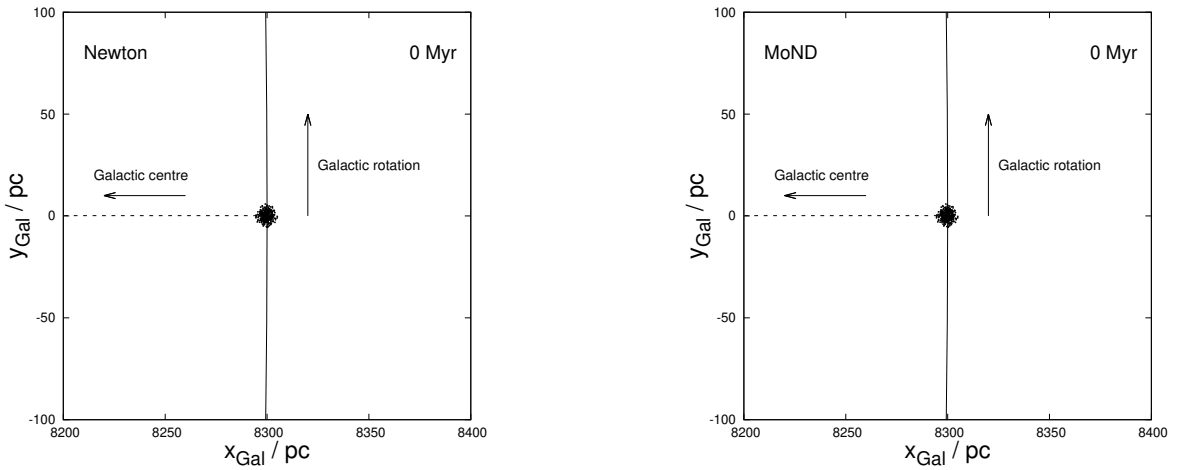


Fig. 14. Orbital snapshots at 0 Myr. Star cluster evolution in Newtonian (left) and discrete Milgrom-law Dynamics (right). See Sect. 5.2 for details.

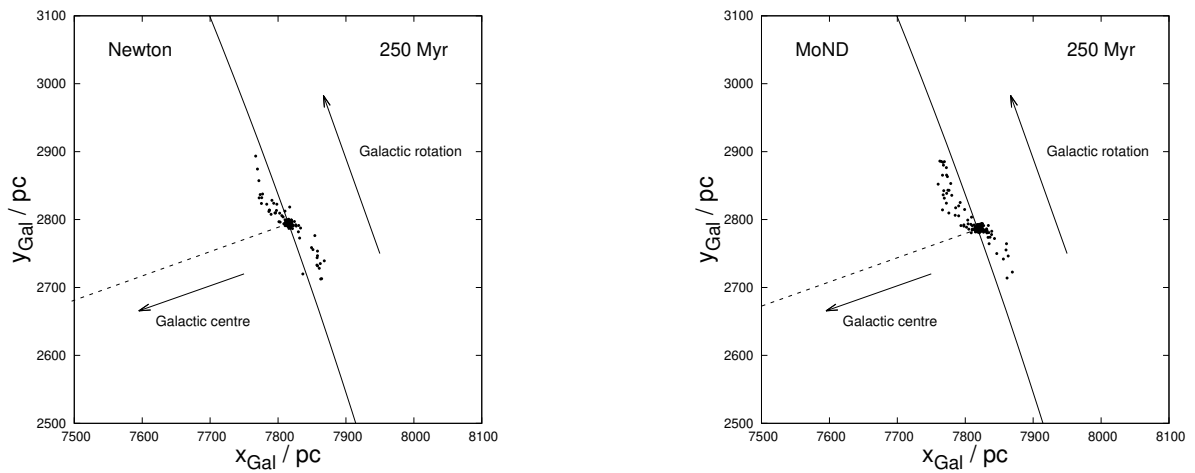


Fig. 15. Same as in Fig. 14 but at 250 Myr.

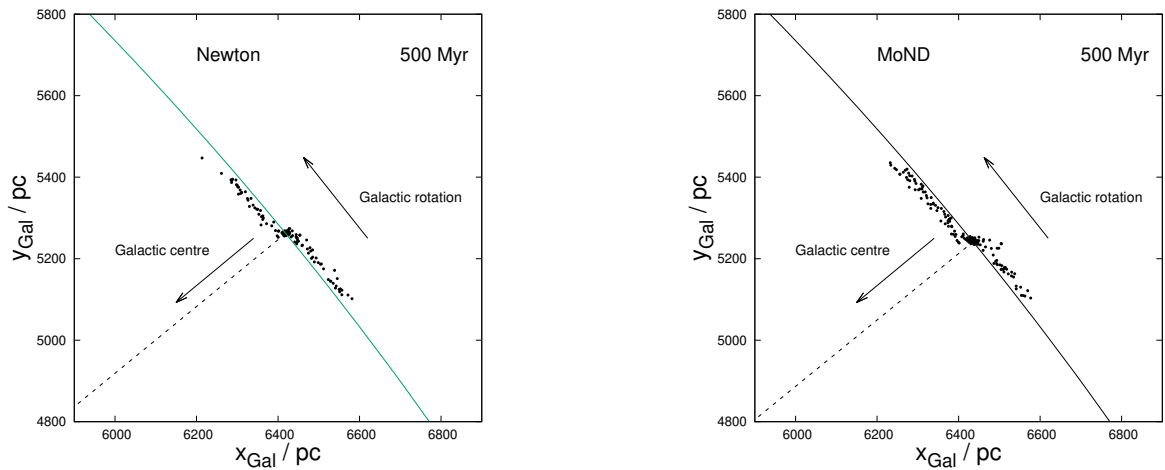


Fig. 16. Same as in Fig. 14 but at 500 Myr.

In the next step the density centre is generally calculated by the weighted sum of all local particle densities (Aarseth 2003). This method requires, that the systems has nearly spherical symmetry. But due to the asymmetric tidal tails this requirement is not met. Therefore, we first determine the position of maximum density,

which is expected to be located close to the centre of the star cluster. Then, only those particles are considered for the calculation of the density centre which lie within a sphere with 10 pc radius where the position of maximum density is at the centre.

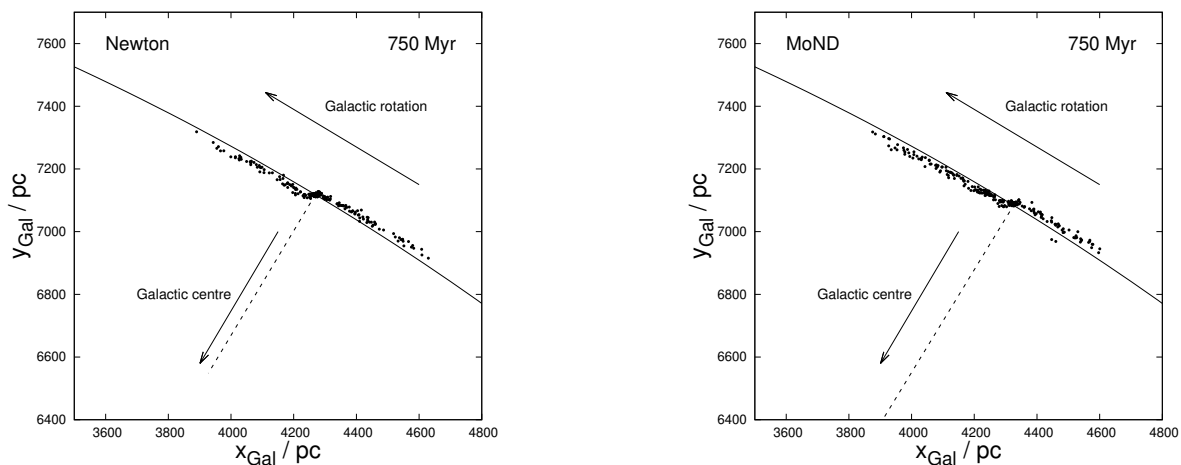


Fig. 17. Same as in Fig. 14 but at 750 Myr.

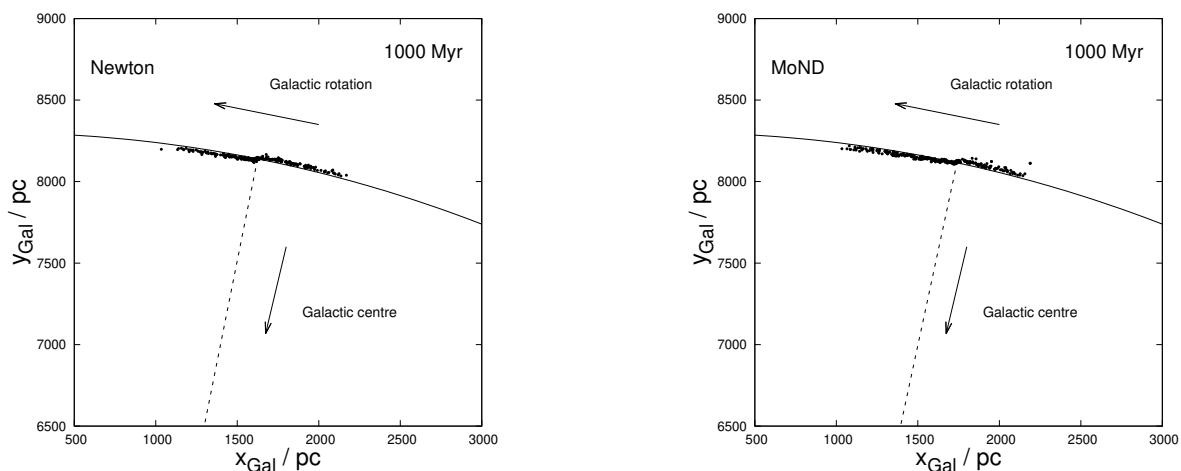


Fig. 18. Same as in Fig. 14 but at 1000 Myr.

5.4. Time evolution of the asymmetry of the tidal tails

The asymmetry of the tidal arms at time t is calculated by

$$\epsilon = \frac{n_l - n_t}{n_l + n_t}, \quad (58)$$

where n_l is the number of stars in the leading arm and n_t is the number of stars in the trailing arm at time t (Pflamm-Altenburg et al. 2023). Thus, for $\epsilon > 0$ the leading arm contains more members than the trailing arm. Fig. 19 shows the evolution of the asymmetry of all 10 simulations. It can be seen that in both dynamical contexts the mean asymmetry is positive, the leading arm contains more members than the trailing arm. But in MONDian dynamics the mean asymmetry varies between 0.2 to 0.3, whereas in Newtonian dynamics the mean asymmetry decreases continuously and slowly below 0.1.

Comparison of the asymmetry of the simulated star clusters with observed star clusters requires that all tidal tail stars of a star cluster can be identified among the field stars. This becomes more difficult with increasing distance of a tidal tail star to the parent star cluster. Therefore, Kroupa et al. (2022) considered only stars within a 50–200 pc distance to the star cluster and introduced the q -parameter

$$q = \frac{N_{l,50-200\text{pc}}}{N_{t,50-200\text{pc}}}, \quad (59)$$

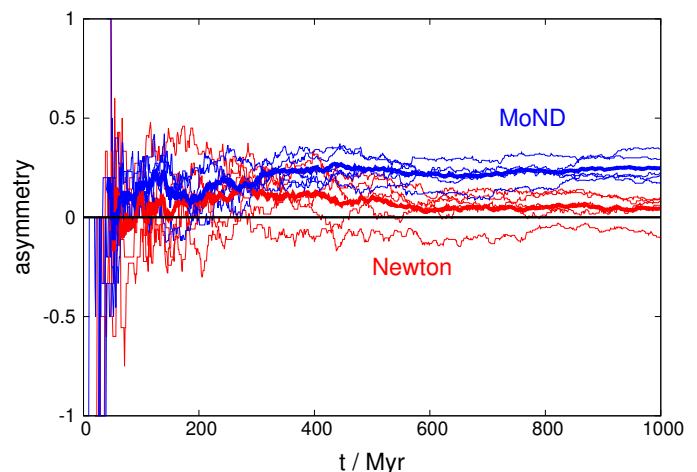


Fig. 19. Asymmetry of tidal arms. Thin lines show the evolution of the asymmetry of the 10 individual simulations, 5 Newtonian (red) and 5 MONDian (blue) simulations. The thick lines show the arithmetic mean values.

where $N_{l,50-200\text{pc}}$ is the number of stars in the leading arm in the considered distance range and $N_{t,50-200\text{pc}}$ the respective number of stars in the trailing arm. For a q -parameter $q > 1$ the leading

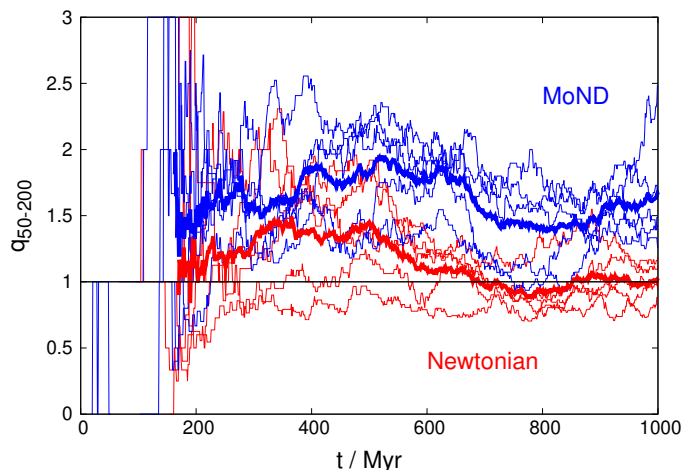


Fig. 20. q -parameter. Thin lines show the evolution of the q -parameter of the 10 individual simulations, 5 Newtonian (red) and 5 MONDian (blue) simulations. The thick lines show the arithmetic mean values.

arm contains more members than the trailing arm in the respective distance range.

The evolution of the q -parameter can be seen in Fig. 20. In MOND the q -parameter varies between 1.5 and 2. The leading arm contains more stars than the trailing arm. In contrast, in Newtonian dynamics the q -parameter finally stays constant around 1 and the tidal tails show no asymmetry.

5.5. Evaporation rate

The number of stars within the constant evaporation radius of 10 pc decrease differently fast in both dynamical theories as shown in Fig. 21. In the MOND model the mean ratio of the current number to the initial number of cluster members after 1 Gyr is 0.26 with a 1σ variance of 0.07. Thus, 74% of the initial stars have already evaporated from the cluster. For 400 initial stars the evaporation rate in the MOND case is 0.296 stars/Myr or one star every 3.4 Myr.

The star cluster evaporates slower in the pure Newtonian case. After 1 Gyr of evolution the mean remaining cluster fraction is 0.41 with a 1σ variance of 0.06. Here, only 59% of all stars have evaporated from the star cluster within 1 Gyr. The evaporation rate is 0.236 stars/Myr or one star every 4.2 Myr. The evaporation rate in the MONDian case is about 25% larger than in the Newtonian case.

This can be understood by the increased effective internal gravitational constant. The external kinematical acceleration of a flat rotation curve with 225 km/s = 230 pc/Myr at a distance of 8300 pc from the galaxy centre is $a_{\text{ext}} = 6.4$ pc/Myr.

For a mass of $\approx 200 M_{\odot}$ and Plummer parameter $b = 3.1$ pc the internal maximal acceleration is 0.036 pc/Myr². Therefore, the internal dynamics is to first order Newtonian with a gravitational constant increased by a factor of $\mu(a_{\text{ext}}/a_0)^{-1} = 1.16$. From Baumgardt & Makino (2003, Eq. 5) it is derived that the dissolution time scale, T_{diss} , of a star cluster in Newtonian dynamics scales inversely with the square root of the gravitational constant, $T_{\text{diss}} \propto G^{-1/2}$. The ratio of the dissolution time scales in the Newtonian case, T_{diss} , and in MLD in case of the external field effect, $T_{\text{diss,EFE}}$, is

$$\frac{T_{\text{diss,EFE}}}{T_{\text{diss}}} = \sqrt{\frac{G}{G_{\text{EFE}}}} = \sqrt{\mu(a_{\text{ext}}/a_0)} = 0.93. \quad (60)$$

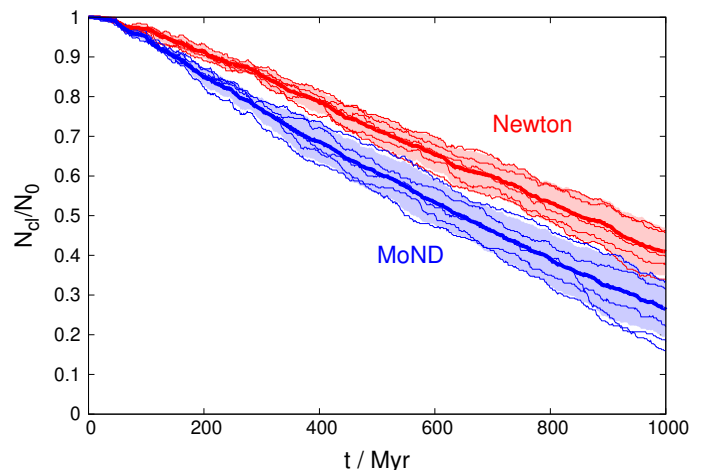


Fig. 21. Evolution of the cluster member number fraction. Each of the 10 models (5 Newtonian (red) and 5 MONDian (blue)) models are shown by thin solid lines. The evolution of the mean values are given by thick solid lines. The light-blue and the light-red areas indicate the 1σ region around the mean value.

The ratio of the numerical dissolution time scale of the models here is approximately

$$\frac{T_{\text{diss,EFE}}}{T_{\text{diss}}} = \frac{\dot{N}}{\dot{N}_{\text{MLD}}} = \frac{0.236}{0.296} = 0.8, \quad (61)$$

and is about 10% smaller than expected from the EFE approximation.

6. Conclusions

Direct N -body simulations of star clusters are performed in a MONDian dynamical context. For this Milgrom's law has been postulated to be valid for arbitrary N -body systems. In comparison to Newton models two main differences emerge: i) The tidal arms are asymmetrically populated. The leading tidal arm contains significantly more stars than the trailing arm. ii) The star cluster evaporates stars or dissolves significantly faster.

The fact that asymmetric tidal tails arise in two different types of MONDian dynamics, that is in QUMOND (Thomas et al. 2018; Kroupa et al. 2022) and Milgrom-law dynamics (this work), leads to the conclusion that this effect is a property of the general MONDian dynamical concept, rather than a result of the detailed realization.

However, the application of Milgrom's law to the dynamics of discrete N -body systems is limited to systems which are internally not Newtonian if embedded in an external MONDian field. This is here artificially achieved by softening the two-body force. Generalized Newtonian equations of motion should already contain internally the non-Newtonianisation of centre of mass motions of compact subsystems, if constructible at all, which needs to be explored.

However, in order to simulate the dynamical evolution of non-relaxed discrete systems like open stars clusters or wide binaries the development of collisional direct N -body codes are required as collision-less methods are not suitable for modeling these kind of systems.

This can be done by deriving mathematically consistent equations of motions for point-mass systems from MOND field theories like AQUAL and QUMOND. But due to the non-linearity this is very difficult to achieve. The other way would be,

to extend the Newtonian equations of motions in such a way that all necessary conditions of MOND-type theories are fulfilled. Both strategies establish a complete new field of research.

Finally, because open star clusters are nearby systems they are very well accessible via astrometric observations, and are ideal test objects to discriminate between the validity of Newtonian or MONDian dynamics on parsec scales.

Acknowledgements. JPA acknowledges permanent hospitality by the Helmholtz-Institut für Strahlen- und Kernphysik.

References

- Aarseth, S. J. 1963, MNRAS, 126, 223
- Aarseth, S. J. 2003, Gravitational N-Body Simulations (Gravitational N-Body Simulations, by Sverre J. Aarseth, pp. 430. ISBN 0521432723. Cambridge, UK: Cambridge University Press, November 2003.)
- Aarseth, S. J., Henon, M., & Wielen, R. 1974, A&A, 37, 183
- Amorisco, N. C., Gómez, F. A., Vegetti, S., & White, S. D. M. 2016, MNRAS, 463, L17
- Aprile, E., Aalbers, J., Agostini, F., et al. 2020, Phys. Rev. D, 102, 072004
- Aprile, E., Abe, K., Agostini, F., et al. 2022, Phys. Rev. Lett., 129, 161805
- Barrena, R., Biviano, A., Ramella, M., Falco, E. E., & Seitz, S. 2002, A&A, 386, 816
- Baumgardt, H. & Makino, J. 2003, MNRAS, 340, 227
- Beccari, G., Jerabkova, T., Boffin, H. M. J., et al. in prep., in preparation
- Bekenstein, J. & Milgrom, M. 1984, ApJ, 286, 7
- Bertone, G. & Hooper, D. 2018, Reviews of Modern Physics, 90, 045002
- Boffin, H. M. J., Jerabkova, T., Beccari, G., & Wang, L. 2022, MNRAS, 514, 3579
- Bonaca, A., Pearson, S., Price-Whelan, A. M., et al. 2020, ApJ, 889, 70
- Bosma, A. 1981, AJ, 86, 1825
- Casertano, S. & Hut, P. 1985, ApJ, 298, 80
- Clowe, D., Bradač, M., Gonzalez, A. H., et al. 2006, ApJ, 648, L109
- Drees, M. 2019, PoS, ICHEP2018, 730
- Erkal, D., Koposov, S. E., & Belokurov, V. 2017, MNRAS, 470, 60
- Ettori, S., Donnarumma, A., Pointecouteau, E., et al. 2013, Space Sci. Rev., 177, 119
- Famaey, B. & McGaugh, S. S. 2012, Living Reviews in Relativity, 15, 10
- Felten, J. E. 1984, ApJ, 286, 3
- Fukushige, T. & Heggie, D. C. 2000, MNRAS, 318, 753
- Hut, P., Makino, J., & McMillan, S. 1995, ApJ, 443, L93
- Ibata, R. A., Lewis, G. F., Thomas, G., Martin, N. F., & Chapman, S. 2017, ApJ, 842, 120
- Jerabkova, T., Boffin, H. M. J., Beccari, G., et al. 2021, A&A, 647, A137
- Knebe, A. & Gibson, B. K. 2004, MNRAS, 347, 1055
- Kokubo, E., Yoshinaga, K., & Makino, J. 1998, MNRAS, 297, 1067
- Kroupa, P., Jerabkova, T., Thies, I., et al. 2022, MNRAS, 517, 3613
- Küpper, A. H. W., Kroupa, P., Baumgardt, H., & Heggie, D. C. 2010, MNRAS, 401, 105
- Lüghausen, F., Famaey, B., & Kroupa, P. 2015, Canadian Journal of Physics, 93, 232
- Makino, J. 1991, ApJ, 369, 200
- Markevitch, M., Gonzalez, A. H., David, L., et al. 2002, ApJ, 567, L27
- Milgrom, M. 1983a, ApJ, 270, 371
- Milgrom, M. 1983b, ApJ, 270, 384
- Milgrom, M. 1983c, ApJ, 270, 365
- Milgrom, M. 1999, Physics Letters A, 253, 273
- Milgrom, M. 2010, MNRAS, 403, 886
- Milgrom, M. 2014, Phys. Rev. D, 89, 024016
- Nusser, A. 2002, MNRAS, 331, 909
- Pearson, S., Price-Whelan, A. M., & Johnston, K. V. 2017, Nature Astronomy, 1, 633
- Pflamm-Altenburg, J., Kroupa, P., Thies, I., et al. 2023, A&A, 671, A88
- Pinfild, D. J., Jameson, R. F., & Hodgkin, S. T. 1998, MNRAS, 299, 955
- Plummer, H. C. 1911, MNRAS, 71, 460
- Read, J. I., Wilkinson, M. I., Evans, N. W., Gilmore, G., & Kley, J. T. 2006, MNRAS, 367, 387
- Röser, S., Schilbach, E., & Goldman, B. 2019, A&A, 621, L2
- Rubin, V. C., Ford, W. K., J., & Thonnard, N. 1978, ApJ, 225, L107
- Teyssier, R. 2002, A&A, 385, 337
- Thomas, G. F., Famaey, B., Ibata, R., et al. 2018, A&A, 609, A44
- Tiongco, M. A., Vesperini, E., & Varri, A. L. 2016, MNRAS, 461, 402